








Strategies to obtain highly ordered deuterated ices presented on the example of ice XIV

Christina M. Tonauser ^a, Elisabet Hauschild ^a, Silvia Eisendle ^a, Violeta Fuentes-Landete ^a, Keishiro Yamashita ^a, Lars Hoffmann ^b, Roland Böhmer ^b and Thomas Loerting ^{a,*}

^aInstitute of Physical Chemistry, University of Innsbruck, Innrain 52c, 6020 Innsbruck, Austria

^bFakultät Physik, Technische Universität Dortmund, Otto-Hahn-Str. 4a, 44227 Dortmund, Germany

*To whom correspondence should be addressed: Email: thomas.loerting@uibk.ac.at

Edited By: Cristina H. Amon

Abstract

Highly ordered deuterated ices have been inaccessible in the past due to the unfavorable slow kinetics. On the example of ice XIV, we introduce three strategies in this study that enhance the degree of order compared with the literature approach of slow cooling. These strategies involve (i) isothermal annealing under pressure, (ii) aging at 77 K, and (iii) introducing isotope defects in addition to the previously used strategy of acid/base doping. We employ the techniques of calorimetry, dielectric relaxation spectroscopy, volumetry, and powder X-ray diffraction to investigate orientational order on the example of the ice XIV–XII order–disorder pair. These strategies allow us to access highly ordered D₂O-ice XIV, tripling the degree of order reached in previous work. These strategies can be employed for other ice phases and hold the potential for future discoveries of new forms of ice with distinct material properties.

Significance Statement

Water ices directly crystallizing from the liquid show a long-range order of oxygen atoms but disordered hydrogen atoms. At low temperatures, hydrogen ordering is thermodynamically favored but often geometrically frustrated. This is especially true for D₂O ices, which are key for structure determination by neutron diffraction. For the ice XII–XIV pair, we present powerful strategies for unlocking the highest degree of order, namely introduction of ionic and Bjerrum point defects, H/D isotope mixing, isothermal pressure annealing, and long-time storage. The new protocol allows for a tripling of the degree of order relative to the previously known weakly ordered ice XIV, where calorimetry, X-ray diffraction, and dielectric spectroscopy data provide clues that highly ordered ice XIV represents a distinct ice polymorph.

Introduction

Since 1998, ices XII–XIX (1–9) and cubic ice without stacking disorder (10, 11) have been discovered—on average, a new ice phase in less than every three years. Recently, ice XX was also proposed (12). In contrast, between the discoveries of ice XI (13) and ice XII (1) >25 years passed, demonstrating that the field of ice physics is more active than ever. A major fruitful driving force has been the search for disorder–order pairs. For four of the newly discovered ordered phases, namely the ices XIII, XIV, XV, and XIX, a disordered counterpart was previously known. In contrast, several other ice phases are still “missing” an ordered counterpart, namely cubic ice, ice IV, ice XVI, and ice XVII. The recent discovery that ice VI has even two differently ordered counterparts (7–9) suggests that for other ices also, a multiplicity of ordered phases may exist. A major obstacle on the way to their discovery are the sometimes extremely slow ordering kinetics (8). Therefore, experimental strategies aimed at accelerating the ordering process of the hydrogen or deuterium atoms in the ice lattice are key for uncovering new ice polymorphs. The present work outlines a new strategy

to achieve this goal and identifies a new candidate for a second ordered polymorph related to ice XII. Yet, the interest in revealing stable and metastable ice polymorphs and, hence, in completing the phase diagram is only one of the reasons to explore different ice phases and their order–disorder transitions. High-pressure ice phases are found in the interior of ice giants, icy moons, and even in the interior of the Earth (14, 15). Ordered and disordered ice phases differ markedly in several properties of practical importance: ordered phases feature vacuum permittivities (dielectric constants) of 2–3, whereas for disordered counterparts, they can exceed 100 (16). Furthermore, disordered phases show plastic flow and high creep: the best-known example is the flow of disordered, hexagonal ice in glaciers. In contrast, ordered phases do not flow and are much more brittle (17, 18). This difference is very important for an understanding of the inner structure of icy moons. There, it is crucial whether ordered ice II or disordered ice III exists at depths in which the pressure is about 0.5 GPa (19, 20). Furthermore, knowledge of how stable hydrogen-bonded networks arrange themselves holds the key for understanding

Competing Interest: The authors declare no competing interest.

Received: November 22, 2023. **Accepted:** November 27, 2023

© The Author(s) 2023. Published by Oxford University Press on behalf of National Academy of Sciences. This is an Open Access article distributed under the terms of the Creative Commons Attribution License (<https://creativecommons.org/licenses/by/4.0/>), which permits unrestricted reuse, distribution, and reproduction in any medium, provided the original work is properly cited.

many-body interactions (21)—and hence, every new ice phase aids in improving intermolecular potentials for computer simulations (22, 23).

In the present work, we study ices XII and XIV, which share the same type of oxygen network. Tetragonal ice XII (space group $I4_2d$) can be made by crystallizing liquid water (1) or by rapidly heating high-density amorphous ice (HDA) (24–26) at pressures between 0.8 and 1.9 GPa. The unique feature of ice XII is a right-handed double helix of water molecules. Orthorhombic ice XIV (space group $P2_12_12_1$) is the hydrogen-ordered phase related to ice XII and was first experimentally identified by Salzmänn et al. (2) with accompanying simulations by Tribello et al. (27). It forms when doped ice XII is slowly cooled to <100 K (2). To accelerate hydrogen ordering, intentional HCl doping is used, which induces point defects on the ice lattice, i.e. Bjerrum L defects and positively charged ionic defects. These defects enhance the reorientation dynamics so that the water molecules retain their mobility down to low temperatures (28–30). Without a dopant, the reorientational dynamics in ice XII are hampered, and below 129 K, the dynamic proton disorder in ice XII freezes into an orientational glass (31), where the H-atom positions remain disordered. HCl doping enhances the dipolar relaxation dynamics by up to four orders of magnitude (28, 32). It has not been fully understood yet why some dopants enhance the hydrogen-ordering process and others do not (33, 34).

However, it is clear that HCl doping increases the dielectric dynamics in ice XII/XIV by four to five orders of magnitude, thereby facilitating the formation of a hydrogen-ordered low-temperature phase (28, 29).

The Pauling entropy ΔS_p represents the difference between the entropies of a fully H-ordered and fully H-disordered ice structure (35). Here, we determine the degree of order using calorimetry and express it as a fraction of ΔS_p . To this end, we integrate the disordering endotherm to obtain the heat of disordering and divide it by the onset temperature T_{onset} of the disordering transition. Assuming quasi-equilibrium conditions (according to the Gibbs–Helmholtz equation), this yields the fraction of Pauling entropy ΔS_p . Our recent work (28, 29) revealed that H_2O -ice XIV can feature two limiting levels of order: about 15–20% of ΔS_p result upon fast cooling, while up to 60% can be reached when slower cooling is employed. Linking this finding to neutron diffraction data, the 15–20% order can be attributed to the partial order of the H6, H9, H11, and H15 sites (2). The crystallographic origin of the 60% ordered ice XIV remains unclear. This high degree of order could not be reached previously for deuterated samples, though. To the best of our knowledge, the highest degree was reported to be about 25% for a D_2O sample cooled at 0.81 GPa at 0.6 K min^{-1} (29). Consequently, previous neutron diffraction studies of ice XIV have suffered from weak ordering of the deuterium atoms (2). From the preparation protocol used in these diffraction experiments (slow cooling at 0.8 K min^{-1} and 0.81 GPa [2]), we estimate the degree of order in the published crystal structure of ice XIV to be about 15–20% of ΔS_p (see Fig. 1c in Fuentes-Landete et al. [29]). This low degree of order is caused by the very slow dynamics of the D-atom sublattice: in deuterated samples, the dielectric dynamics were found to be about 40 times slower than for protiated samples (29). Consequently, it is harder and more time-consuming to reach high degrees of order in deuterated ice XIV.

The aim of the present work is to unravel the factors that govern deuterium ordering in ice XII/XIV. To this end, we infer the degree of deuterium order based on calorimetry and study the reorientational dynamics using dielectric relaxation spectroscopy. We focus on three specific aspects that impact D-ordering:

(i) H/D isotope mixing, (ii) isothermal annealing under pressure, and (iii) aging at 77 K. Item (i) has been successful in accelerating the deuterium dynamics when studying the ordering in the ice VI/XV/XIX trio (7). Here, we will assess whether or not the strategy of introducing faster H-atoms in the bath of D-atoms facilitates D-ordering in the ice XII/XIV system. Item (ii) should help to relax a sample faster than by simple cooling—where the choice of a proper annealing temperature is key. It needs to be high enough to allow for the order to develop at a significant rate, but it needs to be below the equilibrium temperature for the transition between ice XII and ice XIV. For deuterated samples, this temperature is 106 K (29) and so we have chosen 94 K as an annealing temperature. Item (iii) has turned out to be relevant in work on ice XIV since the relaxation times for ice XII/XIV at 77 K are only about 10 days (29). Therefore, the ordering continues slowly, but steadily during sample storage in liquid nitrogen. Here, we quantify the aging effect for ice XIV and exploit it when striving to reach the thermodynamically most stable phase, highly ordered deuterated ice XIV. Furthermore, we also carry out X-ray diffraction measurements to assess changes in the lattice symmetry. Although this technique mainly reveals the oxygen positions, the electric field exerted by the ordered or disordered light atoms can give rise to slight shifts in the O-atom positions. Hence, an increase in order can distort the crystal system from tetragonal ice XII to orthorhombic, monoclinic, or triclinic. This then results in the splitting of several Bragg peaks. Such splittings are not well resolved in laboratory powder X-ray diffraction experiments of weakly ordered ice XIV. However, when using $\text{Cu-K}\alpha$ radiation, for highly ordered H_2O ice XIV, splittings were found at $2\theta = 34.1^\circ$ ($hkl = 310$) and 39.6° ($hkl = 301$) (28, 29).

Results

Deuterium ordering inferred from *in situ* volumetric measurements

First, we compare continuous slow cooling as applied by the previous preparation protocol (2, 28) with the novel protocol involving isothermal annealing by *in situ* volumetry. In both cases, we start with deuterated ice XII (with small amounts of H_2O , as discussed in the *Calorimetric measurements* section), which slowly transforms into ice XIV. Volume changes associated with deuterium ordering detected during continuous cooling to 80 K at 8 K min^{-1} (and 0.81 GPa) are depicted in Fig. 1a and for isothermal annealing at 94 K/0.81 GPa, in Fig. 1b. In both experiments, the ordering of the deuterium atoms can be inferred from a very small (<1%), but detectable change in molar volume. A similar small volume change has been reported near the ice VII/VIII transition (36). In the continuous cooling experiment (see Fig. 1a), ice XII first contracts linearly down to 122 K, but contracts less upon further cooling once ice XIV forms (compare the blue line with the dashed linear extrapolation for XII in Fig. 1a). That is, qualitatively, upon cooling, the thermal contraction of ice XIV is smaller than the one of ice XII. At 94 K, the volume difference ΔV between ice XIV and ice XII is $\sim 1.9 \text{ mm}^3$ (per 600 mg of the sample), assuming linear contraction below $\sim 120 \text{ K}$. For ices I (37), II (38), and III/IX (39), however, a decrease in volume thermal expansion coefficients has been reported in this temperature range. In case of similar behavior of ice XII, this would result in a flattened extrapolated ΔV line and therefore, in a volume difference likely smaller than 1.9 mm^3 between ice XII and ice XIV.

For the isothermal annealing experiment under pressure (see Fig. 1b), the sample was fast-cooled at $p = 0.81 \text{ GPa}$ to 94 K and

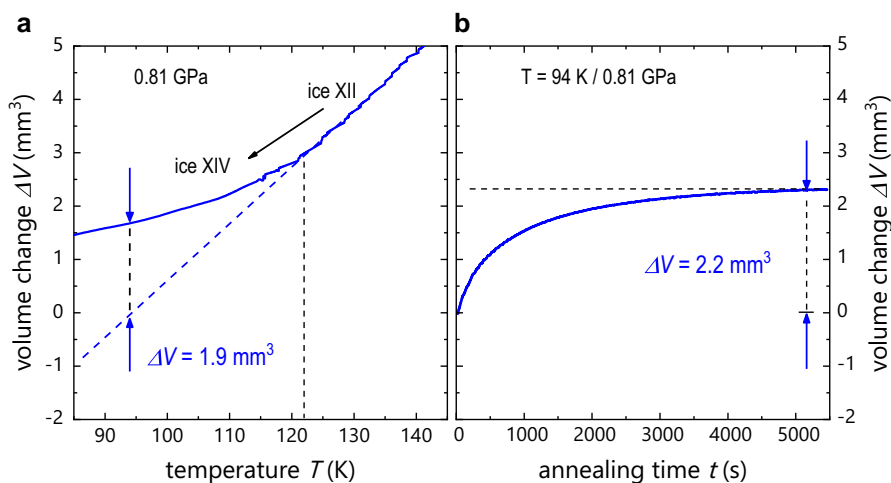


Fig. 1. Volume change accompanying deuterium ordering of ice XII (600 mg, 0.01 DCl, 95% deuterated), i.e. the ice XII → ice XIV transition at 0.81 GPa observed a) upon cooling at 8 K min^{-1} and b) upon isothermal annealing at 94 K. The dashed blue line in a) marks the extrapolated volume change of ice XII upon cooling, assuming (approximately) linear behavior below 122 K. The vertical black dashed line signals the volumetric onset temperature of the ice XII → ice XIV transition. The horizontal black dashed line in b) marks the volumetric convergence for ice XIV formation. For comparing the volume difference between ice XII and ice XIV for the two different preparation protocols, the values at a) 94 K and b) upon reaching convergence are considered (marked by blue vertical arrows).

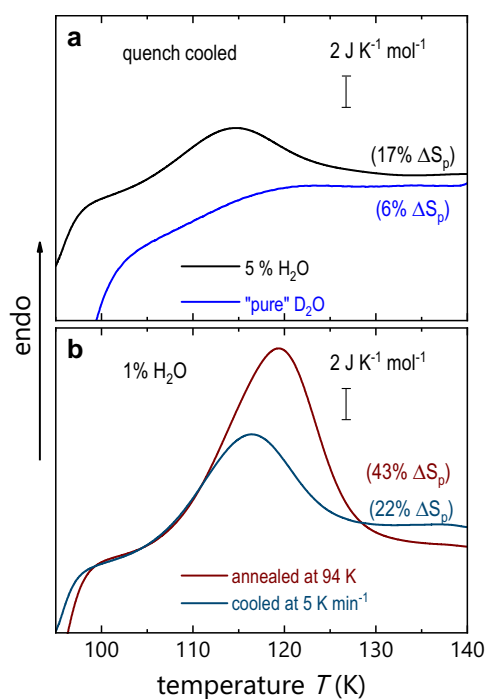


Fig. 2. (a) DSC heating scans of the ice XIV → ice XII transition of an acid-doped sample containing 5% H_2O (top (black) line) compared with a “pure” D_2O sample ($<0.04\% \text{ H}_2\text{O}$, 0.01 M DCl, bottom (blue) line), revealing the promotive effect of H_2O addition on ordering. Because of the extremely weak calorimetric signature of the “pure” D_2O sample, the DSC scan was performed at 50 K min^{-1} (to obtain a stronger heat flow signal), resulting in an onset temperature slightly higher, while all other scans were performed at 30 K min^{-1} . The normalization of the heat flow by the heating rate (and the amount of sample) ensures comparability of the calorimetric signatures. b) DSC scans comparing samples prepared by isothermal annealing (top (dark red) line) and continuous slow cooling (bottom (blue) line), both prepared at 0.81 GPa, containing 1% H_2O .

kept there for 110 min. After fast cooling to 94 K, the sample is still ice XII, since ice XIV has not begun to form, thus defining the starting point. During the subsequent annealing time, an increase in

volume is observed as ice XII transitions to ice XIV. The volume difference between ice XII and ice XIV converges to $\Delta V = +2.2 \text{ mm}^3$ (see blue vertical arrows in Fig. 1b). To check whether this convergence is caused by thermal length changes of the steel pistons, we carried out a blind experiment without any ice sample (see Fig. S1). In this blind experiment, the volume actually decreases, yielding a volume change of $\Delta V = -0.4 \text{ mm}^3$. This means that the volume change caused by the ice XII to ice XIV transition alone amounts to $\Delta V = +2.6 \text{ mm}^3$. The volume difference observed between ice XII and ice XIV at 94 K is larger after isothermal annealing (Fig. 1b) than after continuous slow cooling (Fig. 1a). This suggests that the ice XIV prepared from isothermal annealing under pressure is “more different” from ice XII than the one prepared from continuous slow cooling. Using the 600 mg of ice XII prepared in our experiment and considering a molar volume increase of $1.9 \text{ mm}^3/461 \text{ mm}^3 = +0.41\%$ in Fig. 1a and of $2.6 \text{ mm}^3/461 \text{ mm}^3 = 0.57\%$ at the ice XII/XIV transition in Fig. 1b. The crystallographic densities for ice XII and ice XIV at ambient pressure differ by $+0.46\%$ (2, 41), which is consistent with what we obtain from the continuous cooling protocol. Judging from the volumetric experiment, the ice XIV prepared through isothermal annealing seems to be different from what has been studied previously in neutron diffraction experiments (2). We tentatively assume that this volume increase is related to a higher degree of order and we test this hypothesis in the *Calorimetric measurements* section.

We note that the volume relaxation time for the ice XII/XIV transition can be extracted from Fig. 1b. Defining volume relaxation time as the time it takes for the volume change to reach $1/e$ of the maximum change, we obtain a volume relaxation time of roughly 2,500 s at 94 K and 0.81 GPa.

Calorimetric measurements

Differences in the degree of deuterium order as a function of the preparation protocol can be quantified by the fraction of Pauling entropy ΔS_p , which is accessible by differential scanning calorimetry (DSC). Upon heating the recovered samples, the disordered

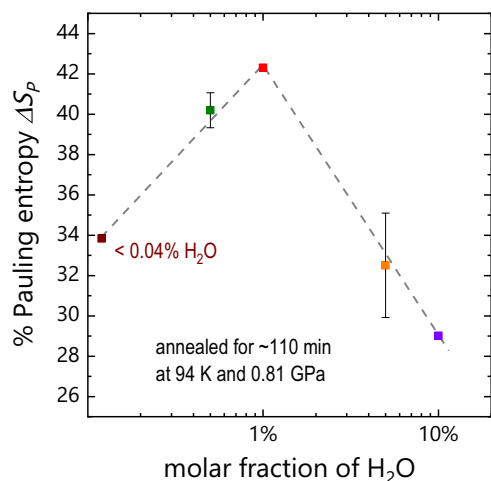


Fig. 3. Fraction of Pauling entropy recovered at the ice XIV → ice XII transition for D_2O samples containing up to 10% H_2O . The raw calorimetry data revealing the D-atom disordering endotherms are shown in Fig. S3. All samples were prepared by annealing for 110 min at 94 K/0.81 GPa. For all samples, DSC analyses were done after 1 to 24 days of storage. The colors of the squares, denoting different isotope mixing ratios, correspond to the ones chosen in Figs. 5, 7, and S3–S5. Entropies are calculated from the integral of the endotherm (i.e. enthalpy) divided by the onset temperature of the ice XIV → ice XII transition. Enthalpy values for the ice XIV → ice XII transition are obtained from comparison with the known literature value for the integral of the ice XII → ice I_{sd} transition exotherm (D_2O : $1,408 \pm 8 \text{ J mol}^{-1}$ [29, 42]). Calculations based on the comparison with the melting endotherm (D_2O : $6,280 \text{ J mol}^{-1}$ [29, 43]) are shown in Fig. S4. We regard the data evaluation shown in Fig. 3 to be more accurate than the one shown in Fig. S4 because the melting endotherm is sometimes afflicted with unwanted evaporation of small droplets from outside the crucible. The dashed line is a guide to the eye.

transition from ice XIV to ice XII can be observed as a pronounced endotherm. Dividing the integrated peak area by the onset temperature T_{onset} (see Fig. S2) yields the fraction of ΔS_p . In the following, the influence of (i) the addition of small amounts of H_2O in D_2O compared with pure D_2O , (ii) isothermal annealing compared with continuous slow cooling (both at 0.81 GPa), and (iii) the amount of H_2O in D_2O on the deuterium ordering in ice XIV shall be presented.

In Fig. 2a, we demonstrate the influence of the addition of small amounts of H_2O , which we refer to as the introduction of isotope defects. This effort is motivated by findings made for the ordering transition from ice VI to ice XIX (7). These observations were rationalized by regarding H-defects in the D-sublattice as fast isotope defects, which then reduce the time it takes for the D-subnetwork to order. Particularly for temperatures below 100 K, it may be speculated that reorientational quantum tunneling is possible for the light H-atom but suppressed for the heavy D-atom. Figure 2a exhibits DSC scans of DCl-doped deuterated samples that were quench-cooled and recovered after the formation of ice XII at 0.81 GPa. That is, the literature protocol for ice XIV formation, i.e. slow cooling $<1 \text{ K min}^{-1}$ at pressures $\geq 0.81 \text{ GPa}$ (2), was intentionally bypassed. For the fully deuterated sample (“pure” D_2O , bottom (blue) line), this procedure—expectedly—results in a very weakly ordered ice XIV sample with merely $\sim 6\%$ ΔS_p . The addition of 5% H_2O , however, leads to a value nearly three (!) times as high (17% ΔS_p , top (black) line). This clearly confirms that the addition of small amounts of H_2O facilitates ordering in ice XII/XIV. Therefore, the samples considered from now on contain small amounts of H_2O , that is, isotope defects.

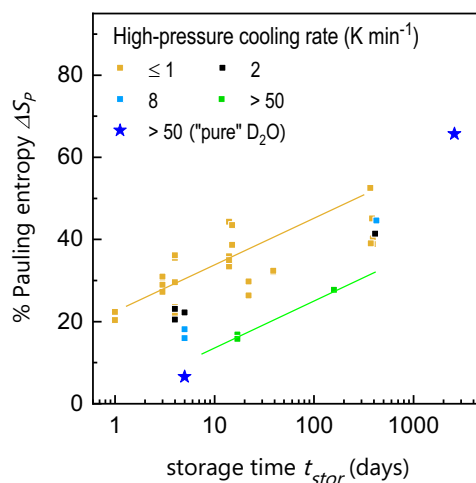


Fig. 4. Impact of storage time (in liquid nitrogen at 77 K and ambient pressure) on the percentage of Pauling entropy observed at the ice XIV → ice XII transition. All symbols—except for the blue asterisks, labeled “pure” (i.e. 99.96%) D_2O —represent samples containing 5% H_2O in D_2O (and 0.01 M DCl). Several samples were repeatedly measured after different storage times. The yellow squares refer to data from several batches of slowly cooled ice XIV ($\leq 1 \text{ K min}^{-1}$), while every other color or symbol refers to an individual sample batch produced at a specific cooling rate as indicated in the legend. To guide the eye, the colored lines are included.

In Fig. 2b, we compare the strategy of continuous cooling vs. isothermal annealing at 0.81 GPa for the preparation of ice XIV samples (containing 1% H_2O). The latent heat associated with deuterium disordering is approximately twice as large for the isothermally annealed samples (top (dark red) line) than for the slowly cooled ones (bottom (blue) line), more precisely 43 vs. 22% Pauling entropy ΔS_p . (Note that after the preparation at elevated pressure [29], prolonged storage in a Dewar at 77 K and ambient pressure further increase the ordering. This aspect is discussed in the *Aging at 77 K and ambient pressure in the Dewar* section). For the annealed samples, the onset temperatures T_{onset} (see Fig. S2) of the ice XIV to ice XII transition are comparable with those of the continuously cooled samples (28, 29). However, it seems that the samples featuring a higher degree of order show a somewhat sharper endotherm and slightly higher onset temperatures. If the degree of ordering exceeds 30%, the onset temperature is $108 \pm 1 \text{ K}$, while it is $106 \pm 1 \text{ K}$ for samples with $\leq 25\%$ order, both for deuterated ice XIV. If this difference is indeed statistically significant, then the implication is that the type of order will be different between highly and weakly ordered ice XIV samples—a hypothesis that we will test further in the *X-ray diffraction* and *Dielectric spectroscopy* sections. For comparison, hydrogenated samples of high order show an onset temperature of $104 \pm 1 \text{ K}$; i.e. the isotope effect on the calorimetric onset temperature is about 4 K.

Figure 3 summarizes the percentage of Pauling entropy observed when adding up to 10% H_2O to D_2O -ice XIV samples prepared by the new isothermal annealing procedure. All samples were prepared with the exact same protocol by annealing for 110 min at 94 K. The degree of deuterium order for the different isotope mixing ratios peaks at about 1% H_2O in D_2O . That is, the addition of less(!) H_2O yields a higher order. In other words, the optimal ratio between fast H-atoms and slow D-atoms is 1:100. Without adding H_2O to the D_2O solution, 33% of order is reached, whereas 45% is reached by adding 1% H_2O . That is, also for ice XII/XIV, small amounts of fast H-defects enhance the dynamics and

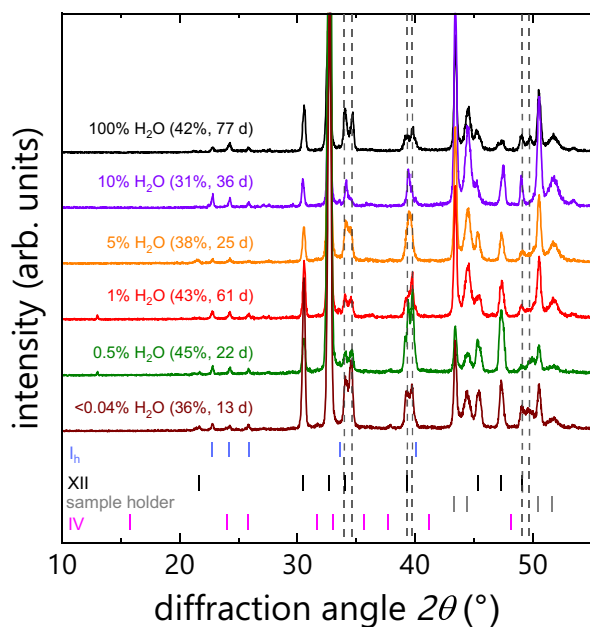


Fig. 5. Powder X-ray diffractograms for highly ordered ice XIV, measured with Cu- $K\alpha$ radiation, compared for different H_2O/D_2O mixing ratios. As indicated by the values in parentheses, these samples feature between 31 and 45% of Pauling entropy, exceeding all literature values on deuterated ice XIV (29). The number of days between sample preparation and calorimetric measurement is also indicated in parentheses. The dashed vertical lines mark Bragg peak splittings that distinguish ice XIV from ice XII. The tick marks refer to the most intense Bragg peaks originating from the sample holder (made from nickel-plated copper), hexagonal ice (I_h), ice IV, and ice XII (1, 41). All measurements were done at >80 K and >0.1 mbar. As best seen from the triplet at $2\theta = 22\text{--}26^\circ$, a tiny amount of hexagonal ice has condensed on the sample while transferring it from liquid nitrogen to the sample holder. For all samples, such contaminations are below 1%. Ice IV, which is the competing phase crystallizing from HDA in parallel with ice XII, also contributes $<1\%$: the most intense ice IV Bragg peak at $2\theta = 31.5^\circ$ is hardly seen in any of the X-ray patterns. The intensity of the most intense Bragg peak of ice XII at $2\theta = 33^\circ$ is more than a factor of 100 higher than the one of ice IV.

the global order. Just like for ice VI/XIX the order–disorder transition temperature is close to 100 K. In future studies, we will test whether this finding also holds for other order–disorder ice pairs with lower order–disorder temperature T_{o-d} , e.g. ice I_h –XI, or higher T_{o-d} , e.g. ices III–IX. The observation that 5 and 10% H_2O additions are actually hindering better ordering has not been noted in our work on ice VI/XIX (8). It seems plausible, though, that there is a limit to the number of fast defects that speed up the global ordering: at some point, with too many fast defects present, their paths frequently cross, thus mutually blocking their fast propagation.

Aging at 77 K and ambient pressure in the Dewar

Yet another factor impacting the degree of deuterium order is how long the samples have been stored in liquid nitrogen after preparation (29). Figure 4 summarizes the percentage of Pauling entropy ΔS_p recovered at the ice XIV/XII transition as extracted from calorimetry scans after different times of storage up to 7 years. Note that we here already employ the “new” strategy of adding small amounts of H_2O (all symbols, except for blue asterisks) to introduce isotope defects but performed the “old” preparation protocol of continuous slow cooling (2, 28). Figure 4 compares samples containing 5% isotope defects that were continuously cooled at high pressures using different cooling rates. This compilation shows that lower cooling rates correspond to higher initial

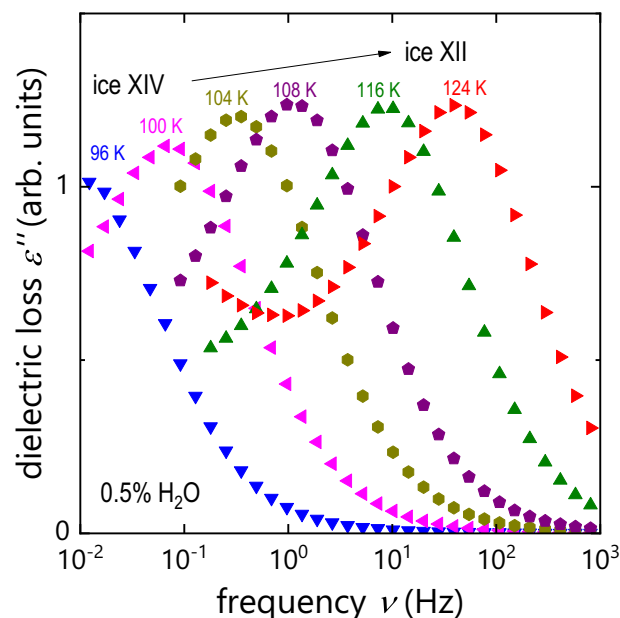


Fig. 6. Dielectric loss spectra for D_2O -ice XIV containing 0.5% H_2O as measured upon heating in the temperature range from 96 to 124 K at the indicated temperatures. The phase transition from ice XIV to ice XII takes place slightly below 104 K.

degrees of order. Samples cooled at >5 K min^{-1} feature $<20\%$ of Pauling entropy when analyzed 1 or 2 weeks after sample preparation. On the other hand, samples cooled at ≤ 1 K min^{-1} reach initial degrees $>30\%$ of ΔS_p a week after preparation.

Figure 4 shows that the degree of order increases with storage time: after 1 day, even at cooling rates ≤ 1 K min^{-1} (yellow squares), no more than $\sim 25\%$ of the Pauling entropy are obtained, whereas after 400 days, it exceeds 40%. The order increases approximately logarithmically in time: the slope of the lines corresponds to a 10% gain in order when increasing the storage time by a factor of 10. For samples cooled at ≤ 1 K min^{-1} (yellow squares), the degree of order increases from $\sim 25\%$ after 4 days to $\sim 30\%$ after 30 days and to $\sim 45\%$ after 400 days. This trend is emphasized using the yellow and green trend lines in Fig. 4. This slope is the same for all the samples containing 5% H_2O (all symbols, except blue asterisks).

For comparison, Fig. 4 contains two data points of a sample without isotope defects (blue asterisks, labeled “pure” [i.e. 99.96%] D_2O). This sample features the lowest order in Fig. 4 shortly after preparation. After 7 years of storage, however, it shows the highest % ΔS_p recovered for any deuterated ice XIV: it has reached 65%. This is fully consistent with earlier findings for H_2O -ice XIV (28, 29). That is, after 7 years of storage also, a D_2O sample without isotope defects reaches the highly ordered state. The impact of isotope defects is to catalyze the ordering, resulting in significant acceleration of the ordering process.

Samples that were prepared using the isothermal annealing under pressure protocol cannot be seen in Fig. 4, simply because none of these samples were remeasured after 1-year storage, so far. Future work has to show whether or not the increase in Pauling entropy proceeds at the same rate as in the continuously cooled samples.

X-ray diffraction

Earlier work on ice XIV has revealed two limits of order in ice XIV, corresponding to a weakly ordered subset prepared at high cooling rates (≥ 50 K min^{-1}) and a highly ordered ice XIV subset prepared

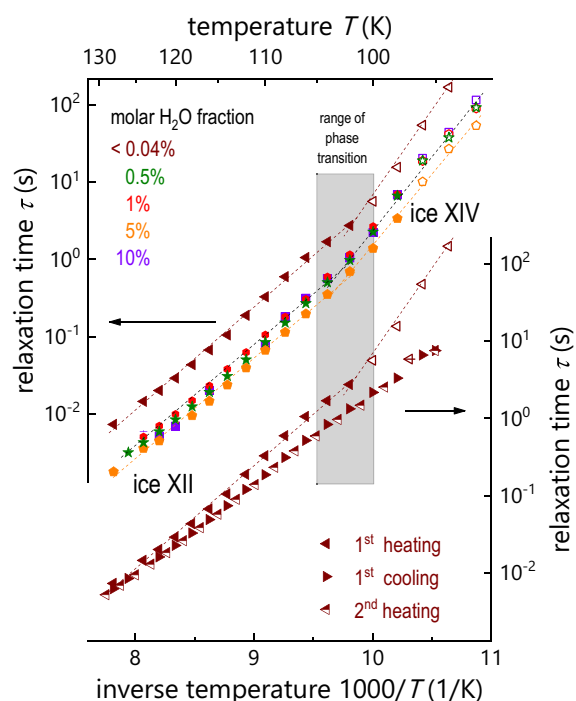


Fig. 7. Arrhenius plots for highly ordered ice XIV samples with different fractions of H₂O as obtained from dielectric loss spectra at ambient pressure such as those shown in Fig. 6. The heating-induced phase transition from ice XIV to ice XII is indicated by the kink in the dashed lines, which guide the eye. Open symbols were determined from peak superposition. The shaded area represents the calorimetrically identified transformation range (Fig. 2). Left and upper axes: a comparison of samples produced using the novel annealing procedure for different molar fractions of H₂O in D₂O. Note that the dynamics for pure, deuterated ice XIV is slower than that of partly hydrogenated ice XIV. Right and lower axes: dielectric relaxation times for an ice XIV sample that was stored for 7 years in liquid nitrogen. Note the pronounced kink in the data near 102 to 104 K for highly ordered ice XIV in the first heating scan. After transformation to ice XII, the sample is recooled (first cooling) to produce weakly ordered ice XIV and then reheated (second heating). Note the absence of a kink for weakly ordered ice XIV.

at lower cooling rates (29). Previous attempts to produce highly ordered deuterated ice XIV were not successful. At most 30% ΔS_p , see Fig. 3c in Fuentes-Landete et al. (29), could be attained using a continuous cooling protocol. Even ambient-pressure cooling rates as low as 0.01 or 1 K min⁻¹ at 0.81 GPa only produce 30% order (29). The novel annealing protocol developed for the present work allows us to go beyond that. We now reach between 30 and 45% order after <2 months of storage. The volumetric difference of 0.6% between ice XII and ice XIV as reported in Fig. 1 suggests that these ice phases might feature a slightly different oxygen atom network. This suggestion is probed on the basis of powder X-ray diffraction patterns recorded at 80 K using Cu-K α radiation (see Fig. 5).

Powder diffraction patterns for weakly ordered deuterated ice XIV samples featuring 3–24% order are reported in Fig. 5 of Köster et al. (28). These patterns do not provide evidence for any splitting of ice XII Bragg peaks—they are practically identical to those for ice XII and for weakly ordered ice XIV. Only for 24% ordering, an asymmetry develops for the Bragg peaks at $2\theta = 34.1^\circ$ and 39.6° . The present work reports powder patterns for samples made using the novel isothermal annealing protocol. In contrast to the earlier work, Fig. 5 reveals well-defined splittings for the Bragg peaks at $2\theta = 34.1^\circ$, 39.6° , and 49.1° , highlighted by the

vertical dashed lines. These correspond to the singlet Bragg peaks of 310, 301, and 420 in ice XII, whose splittings accompanying additional 130, 031, and 240 peaks in ice XIV indicate that ice XIV is no longer tetragonal. Possibly, there is also a splitting at $2\theta = 47.3^\circ$ ($hkl = 112$), which can imply that highly ordered ice XIV is less symmetric than orthorhombic, such as monoclinic or triclinic. Such hints for this splitting can be seen for the 1% H₂O and the 100% H₂O sample in Fig. 5, but the evidence is not conclusive so far. However, such splittings hint at the possibility of a crystallographic difference between weakly and highly ordered ice XIV. The splittings at $2\theta = 34.1^\circ$ and 39.6° were previously also identified for highly ordered H₂O-ice XIV samples (see Fig. 5 in Köster et al. [28]). The splitting marked in Fig. 5 at $2\theta = 49.1^\circ$ could not be resolved, so far, not even for 60% ordered H₂O-ice XIV (28). However, here we do observe this splitting for an H₂O sample of 42% order (top trace in Fig. 5). The origin of the difference could be related to texture/preferred orientation effects or to a different nature of ice XIV prepared through isobaric annealing. Inspecting Fig. 5 more carefully, the splittings are resolved best for pure H₂O-ice XIV and also for D₂O samples containing <1% H₂O. The two samples containing 5 or 10% H₂O display only weak shoulders for the $2\theta = 34.1^\circ$ and 39.6° peaks. Samples with higher ordering (see the previous section) show a clearer peak splitting. These observations regarding the Bragg peak splittings correlate well with the order maximum at 1% H₂O in Fig. 3 and support the view that highly ordered ice XIV is indeed different from weakly ordered ice XIV.

Dielectric spectroscopy

As suggested above, the high order achieved for ice XIV in the present work is enabled by the changed protocol and because of the addition of fast H-defects via small amounts of H₂O to the D₂O solution. Next, we examine whether the impact of these fast defects can be detected in the dielectric relaxation dynamics. Fuentes-Landete et al. have shown that in the absence of point-defect doping, the dielectric relaxation dynamics in deuterated ice XII are about one decade slower than in hydrogenated ice XII (29). Acid doping accelerates the relaxation dynamics by about four decades for both isotopes (28). In the present work, we investigate the additional impact of partial isotopic replacement on samples containing intentional hydrogen atom defects, i.e. we test our hypothesis regarding the fast isotope defects in ice XIV. Specifically, DCl-doped D₂O samples containing 10, 5, 1, 0.5, and <0.04% H₂O were measured. Figure 6 shows the dielectric loss spectra of samples containing 0.5% H₂O in D₂O for temperatures between 96 and 124 K. With increasing temperature, the peak frequencies ν_{\max} of the spectra shift to higher frequencies. Below about 102 K, the T-induced spectral shift is much more pronounced than for higher temperatures. This changed behavior is indicative of the phase transition from ice XIV to ice XII taking place slightly above 102 K.

Based on the dielectric peak loss frequencies, the temperature-dependent dielectric relaxation time $\tau_{\max} = (2\pi \nu_{\max})^{-1}$ is calculated and plotted as filled symbols in an Arrhenius plot, see the upper part of Fig. 7. Open symbols are determined from a frequency-temperature-superposition analysis (44), i.e. the spectra devoid of a visible peak were shifted along the logarithmic frequency axis to achieve overlap with spectra displaying a peak. From the shift factors, relaxation times are deduced, thus enabling us to extend the accessible range of time scales. There is a kink in the linear $\tau(T)$ trend (dashed lines) between 102 and 104 K which reflects the phase transition between ice XII and ice XIV. The

observed transition is about 5 K lower than in the calorimetry experiment (103 vs. 108 K). This difference is kinetic in origin, since the heating rate employed in the dielectric relaxation measurement (on average 6 K h^{-1}) is much smaller than the one used for the calorimetry scans (30 K min^{-1}). Similar observations were previously made for the transition of low-density amorphous ice (45), ice IV (28), ice V (32), ice VI (28), and ice XII (30) to stacking-disordered ice or for the disordering temperature of ice XIX (8).

Among the five different isotopic compositions investigated in the present work, nominally pure D_2O ($<0.04\% \text{ H}_2\text{O}$) clearly shows the largest relaxation times, i.e. the slowest relaxation (brown triangular symbols in Fig. 7). The relaxation times are shifted by more than half a decade to lower values for all samples containing small amounts of H_2O (0.5, 1, 5, and 10%). The dynamics in the samples with 5 and 0.5% H_2O addition seem to be slightly faster than for the other compositions. This is also recognized when comparing the relaxation spectra isothermally, e.g. at 102 K, just below the transition temperature to ice XII (see Fig. S5). The 0.5 and 5% H_2O -containing samples show the highest peak frequencies ν_{max} . While for all ice XIV samples with added H_2O , the dynamics are resolved in the present frequency window; in nominally pure D_2O , it is so slow that a peak maximum is not directly observable.

The finding from calorimetry and X-ray diffraction that 5 and 10% hydrogenated samples produce less global order in ice XIV than those with 0.5 and 1% (see Fig. 3) is not reflected in the dielectric measurements. It is tempting to speculate that this difference can be traced back to the fact that dielectric relaxation spectroscopy probes the dynamics of the initial step of reorientation (rotation of the water molecule or hop of an H atom from one O atom to the next neighbor) and that, in contrast, X-ray and calorimetry assess the global order. The development of the latter requires not only fast initial reorientation but also defect propagation through the network. This propagation might be hindered if the number of fast H-defects is too large (34). The volume relaxation time of 2,500 s at 94 K, see Fig. 1, compares with a dielectric relaxation time of about 100 s at 94 K. This difference similarly suggests that dielectric relaxation only probes the initial reorientation step, whereas volume relaxation requires the initial step *plus* propagation through the network.

Finally, in the lower part of Fig. 7, we compare the dielectric relaxation time scales of highly ordered ice XIV with those of weakly ordered ice XIV. To this end, we used the ice XIV sample that was stored for 7 years in the Dewar, showing 65% D-order. This highly ordered ice XIV was slowly heated to 130 K at ambient pressure, thus transforming it into ice XII. Immediately thereafter, the sample was cooled down, producing weakly ordered ice XIV. Based on our earlier work (29), the degree of ordering in the weakly ordered ice XIV formed in this process is estimated to be only $\sim 5\%$. This weakly ordered ice XIV is heated up a second time. For highly ordered ice XIV (first heating scan), the transition to ice XII is signaled by a pronounced kink, whereas a kink is absent for weakly ordered ice XIV (second heating scan), see Fig. 7. The relaxation times recorded during the second heating essentially reproduce those obtained during the prior cooling. This finding implies that in highly ordered ice XIV, the dielectric relaxation dynamics are clearly slower than in weakly ordered ice XIV. At 95 K, the difference is about one order of magnitude. That is, the D-bond network is stiffer and relaxes more slowly in highly ordered than in weakly ordered ice XIV, compatible with the expectation that highly ordered ice XIV is thermodynamically more stable than weakly ordered ice XIV.

Conclusions

In the present work, we study deuterium ordering in the high-pressure polymorph ice XII, transforming it to ice XIV. In the past, about 60% of hydrogen order could be obtained in H_2O -ice XIV (28) and no more than 25% of deuterium order in D_2O -ice XIV (29). Here, we are able to access highly ordered (up to 65%) D_2O -ice XIV using a novel preparation protocol. First, this involves isothermal annealing of the ice XII sample at 0.81 GPa and 94 K for 110 min, which is below the order–disorder temperature $T_{\text{o-d}}$ at 103 K as determined from very slow heating experiments using dielectric relaxation spectroscopy at ambient pressure. In much faster calorimetry scans, a transition from ice XIV to ice XII is observed at T_{onset} of 108 K. In the 110 min of high-pressure annealing, the deuterium atoms order much more than by slow cooling of ice XII to $T < T_{\text{o-d}}$. Procedures involving more or less slow cooling were employed in all earlier work on ice XIV, either at ambient pressure or under high-pressure conditions (29). Remarkably, in contrast to earlier dilatometry studies on ice, volumetric measurements enable us to monitor the process of ordering. The volumetric measurements reveal a density difference of about 0.6% between highly ordered ice XIV and ice XII. This density difference exceeds the density difference between ice XII and weakly ordered ice XIV from diffraction studies (2, 41), hinting at a crystallographic difference between highly and weakly ordered ice XIV. Based on calorimetry, this novel annealing protocol approximately doubles the degree of order and moreover is much more time efficient than earlier preparation procedures (2, 28, 29).

A second aspect that helps in preparing highly ordered deuterated ice XIV is the addition of a small amount of H_2O to D_2O . This introduces fast H-atoms into the sublattice of slow D-atoms. About 0.5% H_2O addition is sufficient to increase the dielectric relaxation dynamics by a factor of 10 and to increase the calorimetrically inferred order by about 10% of ΔS_{p} right after preparation. This observation is similar to earlier ones regarding the ordering from ice VI to ice XIX (7). These equivalent consequences raise the possibility that the presently pursued strategy will facilitate deuterium ordering also for other ice phases. We suspect that the rather low disordering temperature near 100 K found for both ice XIV and ice XIX might be essential to rationalize the isotope effect in the ordering kinetics and conjecture that quantum tunneling of H-atoms might be the decisive factor enhancing the H-atoms kinetics over those of the D-atoms.

Third, here we show that the degree of deuterium order in weakly ordered ice XIV can also be enhanced through sample storage at 77 K: in quantitative terms, the degree of ordering increases by 10% when increasing the storage time by a factor of 10. For a deuterated ice XIV sample stored for 7 years, we recover 65% of the Pauling entropy—even more than previously accessible in protiated ice XIV (28).

We call the presently obtained samples “highly ordered ice XIV.” Earlier work on H_2O -ice XIV (28, 29) revealed two distinct time scales for H-ordering, where the limit of weak ordering (near 20% of the Pauling entropy) was easily accessible, but the limit of high ordering (near 60%) could be accessed only in very time-demanding experiments involving slow cooling (28). For deuterated ice XIV, we now also reach or even exceed the higher limit (65% for the sample stored for 7 years). These highly ordered ice XIV samples differ from weakly ordered ice XIV not only in terms of calorimetrically inferred order but also in terms of volumetrically determined density. In powder X-ray diffractograms, highly ordered ice XIV differs from ice XII and ice XIV in terms of clear peak splittings for three Bragg peaks, while weakly ordered ice

XIV is very similar to ice XII. Future work needs to show whether there is a crystallographic difference between highly and weakly ordered ice XIV and to determine whether highly ordered ice XIV is actually an ice phase different from both ice XII and ice XIV. The dielectric experiments corroborate this suspicion: at $T < 102$ K, highly ordered ice XIV relaxes by about one order of magnitude slower than weakly ordered ice XIV. This suggestion of highly ordered ice XIV being a novel ice phase needs to be tested by neutron diffraction. In previous neutron diffraction work, merely the crystal structure of (weakly ordered) D_2O -ice XIV was established (2). The present study clarifies the decisive step in producing highly ordered deuterated ice XIV in significant quantities in a relatively short time—making neutron diffraction studies possible in future work. Furthermore, the strategies proposed in this study for enhancing deuterium ordering in XIV, i.e. isothermal annealing under pressure, introduction of isotope defects in addition to acid/base doping, and aging at 77 K can be applied to other order-disorder pairs to explore the possibilities for alternative ordering as it was first shown for the ice VI/XV/XIX triplet (7, 9). The present work on deuterated ice XIV clearly shows the polymorphic phase transition behavior to be different for highly and weakly ordered ice XIV, making the case that we successfully produced an ice phase with properties distinct from all ices reported in the literature.

Experimental methods

Sample preparation and volumetric measurements

To produce ice XIV, ice XII samples are prepared by crystallizing HDA ice in a piston-cylinder setup. Following the protocol of Mishima et al. (46), HDA is made by freezing liquid water at ambient pressure and subsequent pressurization of the resulting hexagonal ice to 1.6 GPa at 77 K. By isobaric heating at >25 K min^{-1} and 0.81 GPa to 200 K, HDA crystallizes to ice XII. The high heating rates suppress the competing crystallization to ice IV, and pure ice XII forms (28, 29, 31). The ice samples were compressed in a computerized universal testing machine (Zwick, model BZ100/TL3S) featuring a piston cylinder and an 8-mm bore. To avoid pressure drops and shockwave heating during compression, indium containers were used. All samples were prepared from 600 μL of water with different isotopic compositions and either 0.01 M DCl (for mainly D_2O solutions) or 0.01 M HCl (H_2O). The H_2O mole fractions employed here are <0.04 , 0.5, 1, 5, and 10% H_2O in D_2O as well as 100% H_2O .

Differential scanning calorimetry

To analyze the degree of deuterium ordering, calorimetric measurements were performed with a differential scanning calorimeter (DSC8000 Perkin Elmer). As in previous works (28, 29, 31), the samples were transferred to aluminum crucibles under liquid nitrogen and cold loaded into the instrument. Ambient-pressure heating scans were conducted with 30 K min^{-1} . The scans of D_2O -ice XIV samples show three first-order transitions: an endotherm due to the order-disorder transition from ice XIV to ice XII at $T_{\text{onset}} \approx 108$ K, an exotherm at $T_x \approx 158$ K signaling the polymorphic transition from ice XII to stacking-disordered ice I_{sd} , and finally, the melting endotherm of hexagonal ice at $T_m \approx 277$ K. As in earlier work (28, 29), the Pauling entropy is deduced in two ways: from the area ratio of the ice XIV \rightarrow XII endotherm to the ice XII $\rightarrow I_{\text{sd}}$ exotherm and alternatively from the ice XIV \rightarrow XII endotherm to the melting endotherm ($I_{\text{h}} \rightarrow$ liquid water)

where only the latent heat for the ice XIV \rightarrow XII endotherm is unknown and the other latent heats are taken from literature (42, 47).

X-ray diffraction

Powder X-ray diffraction was used to check the ice XII/XIV samples for distortions of the ice XII oxygen lattice that are mediated through the ordering of the D-atoms. Distortions typically lower the symmetry and, compared with the disordered parental phases, produce Bragg peak splittings in ordered phases. The X-ray diffraction measurements also serve to check for unwanted by-phases, especially ice IV, which can crystallize from HDA in parallel to ice XII when the high-pressure heating rates are too low (26, 48). When quickly transferring the cold samples to the sample holder through humid air, small quantities of hexagonal ice may condense on the sample surface and may appear as contamination in the powder patterns. The X-ray measurements were conducted at 0.1 mbar and $T \approx 80$ K with a Siemens D5000 diffractometer (Cu-K α , $\lambda = 1.5406$ Å) in θ - θ geometry. The sample preparation and loading procedures were carried out according to well-established methods (29, 32).

Dielectric spectroscopy

As a fourth analytic method, dielectric measurements were carried out on the deuterated ice samples. Powdered samples were cold-loaded into a parallel-plate capacitor made of invar and sapphire (49) and mounted into a cryostat. Broadband dielectric spectra were recorded using an Alpha Analyzer for frequencies between 2×10^{-2} and 10^4 Hz and temperatures from 90 to 295 K at ambient pressure. The temperature was adjusted with a nitrogen gas flow and stabilized within ± 0.1 K through a Quatro Temperature Controller. Temperature steps were set at 2 K up to 130 K, 3 K up to 150 K, and 5 K for higher temperatures. Like in earlier work (32), the dielectric measurements were primarily exploited to extract dielectric relaxation times from the dielectric loss peak frequencies.

Supplementary Material

Supplementary material is available at PNAS Nexus online.

Acknowledgements

This research was supported by the Centre for Molecular Water Science (CMWS, DESY Hamburg) in an Early Science Project. C.M.T. was a recipient of a DOC fellowship from the Austrian Academy of Sciences (ÖAW) and was supported by the Early Stage Funding 2021 of the University of Innsbruck.

Author Contributions

C.M.T., R.B., and T.L.: designed the research; C.M.T., E.H., S.E., V.F.-L., and L.H.: performed the research; C.M.T., E.H., S.E., L.H., K.Y., R.B., and T.L.: analyzed the data; C.M.T., E.H., R.B., and T.L.: wrote the paper.

Preprints

An earlier version of this manuscript was posted on a preprint server (Research Square: <https://doi.org/10.21203/rs.3.rs-1908887/v1>).

Data Availability

The data underlying this article are available in the article and in its [supplementary material](#).

References

- Lobban C, Finney JL, Kuhs WF. 1998. The structure of a new phase of ice. *Nature*. 391:268–270.
- Salzmann CG, Radaelli PG, Hallbrucker A, Mayer E, Finney JL. 2006. The preparation and structures of hydrogen ordered phases of ice. *Science*. 311:1758–1761.
- Salzmann CG, Radaelli PG, Mayer E, Finney JL. 2009. Ice XV: a new thermodynamically stable phase of ice. *Phys Rev Lett*. 103:105701.
- Falenty A, Hansen TC, Kuhs WF. 2014. Formation and properties of ice XVI obtained by emptying a type sII clathrate hydrate. *Nature*. 516:231–233.
- del Rosso L, Celli M, Ulivi L. 2016. New porous water ice metastable at atmospheric pressure obtained by emptying a hydrogen-filled ice. *Nat Commun*. 7:13394.
- Millot M, et al. 2019. Nanosecond X-ray diffraction of shock-compressed superionic water ice. *Nature*. 569:251–255.
- Gasser TM, Thoeny AV, Fortes AD, Loerting T. 2021. Structural characterization of ice XIX as the second polymorph related to ice VI. *Nat Commun*. 12:1128.
- Gasser TM, et al. 2018. Experiments indicating a second hydrogen ordered phase of ice VI. *Chem Sci*. 9:4224–4234.
- Yamane R, et al. 2021. Experimental evidence for the existence of a second partially-ordered phase of ice VI. *Nat Commun*. 12:1129.
- Komatsu K, et al. 2020. Ice I_c without stacking disorder by evacuating hydrogen from hydrogen hydrate. *Nat Commun*. 11:464.
- Del Rosso L, et al. 2020. Cubic ice I_c without stacking defects obtained from ice XVII. *Nat Mater*. 19:663–668.
- Prakapenka VB, Holtgrewe N, Lobanov SS, Goncharov AF. 2021. Structure and properties of two superionic ice phases. *Nat Phys*. 17:1233–1238.
- Kawada S. 1972. Dielectric dispersion and phase transition of KOH doped ice. *J Phys Soc Jpn*. 32:1442–1442.
- Encrenaz T. 2008. Water in the solar system. *Annu Rev Astron Astrophys*. 46:57–87.
- Tschauner O, et al. 2018. Ice-VII inclusions in diamonds: evidence for aqueous fluid in Earth's deep mantle. *Science*. 359:1136–1139.
- Wilson GJ, Chan RK, Davidson DW, Whalley E. 1965. Dielectric properties of ices II, III, V, and VI. *J Chem Phys*. 43:2384–2391.
- Petrenko VF, Whitworth RW. 1999. *Physics of ice*. Oxford, New York: Oxford University Press.
- Durham WB, Kirby SH, Stern LA. 1997. Creep of water ices at planetary conditions: a compilation. *J Geophys Res*. 102:16293–16302.
- Durham W, Stern L. 2001. Rheological properties of water ice—applications to satellites of the outer planets. *Annu Rev Earth Planet Sci*. 29:295–330.
- Kubo T, Durham WB, Stern LA, Kirby SH. 2006. Grain size-sensitive creep in ice II. *Science*. 311:1267–1269.
- Engel EA, Anelli A, Ceriotti M, Pickard CJ, Needs RJ. 2018. Mapping uncharted territory in ice from zeolite networks to ice structures. *Nat Commun*. 9:2173.
- Babin V, Leforestier C, Paesani F. 2013. Development of a “first principles” water potential with flexible monomers: dimer potential energy surface, VRT spectrum, and second virial coefficient. *J Chem Theory Comput*. 9:5395–5403.
- Abascal JLF, Sanz E, García Fernández R, Vega C. 2005. A potential model for the study of ices and amorphous water: TIP4P/ice. *J Chem Phys*. 122:234511.
- Loerting T, Kohl I, Salzmann C, Mayer E, Hallbrucker A. 2002. (Meta-)stability domain of ice XII revealed between ≈ 158 –212 K and ≈ 0.7 –1.5 GPa on isobaric heating of high-density amorphous ice. *J Chem Phys*. 116:3171–3174.
- Kohl I. 2001. *High density amorphous ice and its phase transition to ice XII [doctoral thesis]*. [Austria]: University of Innsbruck.
- Salzmann CG, Kohl I, Loerting T, Mayer E, Hallbrucker A. 2003. Pure ices IV and XII from high-density amorphous ice. *Can J Phys*. 81:25–32.
- Tribello GA, Slater B, Salzmann CG. 2006. A blind structure prediction of ice XIV. *J Am Chem Soc*. 128:12594–12595.
- Köster KW, et al. 2015. Dynamics enhanced by HCl doping triggers 60% Pauling entropy release at the ice XII–XIV transition. *Nat Commun*. 6:7349.
- Fuentes-Landete V, Köster KW, Böhmer R, Loerting T. 2018. Thermodynamic and kinetic isotope effects on the order–disorder transition of ice XIV to ice XII. *Phys Chem Chem Phys*. 20:21607–21616.
- Plaga LJ, et al. 2019. Amorphous and crystalline ices studied by dielectric spectroscopy. *J Chem Phys*. 150:244501.
- Salzmann CG, Kohl I, Loerting T, Mayer E, Hallbrucker A. 2003. The low-temperature dynamics of recovered ice XII as studied by differential scanning calorimetry: a comparison with ice V. *Phys Chem Chem Phys*. 5:3507.
- Köster KW, et al. 2016. Doping-enhanced dipolar dynamics in ice V as a precursor of hydrogen ordering in ice XIII. *Phys Rev B*. 94:184306.
- Salzmann C, Radaelli P, Hallbrucker A, Mayer E, Finney J. 2007. 11th International Conference on the Physics and Chemistry of Ice 521:528.
- Köster KW, Klocke T, Wieland F, Böhmer R. 2017. Interplay of defect doping and Bernal-Fowler rules: a simulation study of the dynamics on ice lattices. *Phys Rev B*. 96:134301.
- Pauling L. 1935. The structure and entropy of ice and of other crystals with some randomness of atomic arrangement. *J Am Chem Soc*. 57:2680–2684.
- Kuhs WF, Finney JL, Vettier C, Bliss DV. 1984. Structure and hydrogen ordering in ices VI, VII, and VIII by neutron powder diffraction. *J Chem Phys*. 81:3612–3623.
- Fortes AD. 2018. Accurate and precise lattice parameters of H₂O and D₂O ice I_h between 1.6 and 270 K from high-resolution time-of-flight neutron powder diffraction data. *Acta Crystallogr B Struct Sci Cryst Eng Mater*. 74:196–216.
- Fortes AD, Wood IG, Alfredsson M, Vočadlo L, Knight KS. 2005. The incompressibility and thermal expansivity of D₂O ice II determined by powder neutron diffraction. *J Appl Crystallogr*. 38:612–618.
- Tanaka H, Matsumoto M, Yagasaki T. 2022. On the role of intermolecular vibrational motions for ice polymorphs. IV. Anisotropy in the thermal expansivity and the nonaffine deformation for ice IX and III. *J Chem Phys*. 157:174505.
- Loerting T, et al. 2011. Cryoflotation: densities of amorphous and crystalline ices. *J Phys Chem B*. 115:14167–14175.
- Koza M, Schober H, Tölle A, Fujara F, Hansen T. 1999. Formation of ice XII at different conditions. *Nature*. 397:660–661.
- Salzmann CG, Mayer E, Hallbrucker A. 2004. Thermal properties of metastable ices IV and XII: comparison, isotope effects and relative stabilities. *Phys Chem Chem Phys*. 6:1269.

- 43 Long EA, Kemp JD. 1936. The entropy of deuterium oxide and the third law of thermodynamics. Heat capacity of deuterium oxide from 15 to 298°K. The melting point and heat of fusion. *J Am Chem Soc.* 58:1829–1834.
- 44 Stern J, et al. 2015. Experimental evidence for two distinct deeply supercooled liquid states of water—response to “comment on ‘Water’s second glass transition’”, by G.P. Johari, *Thermochim Acta* (2015). *Thermochim Acta.* 617:200–207.
- 45 Lemke S, et al. 2017. Relaxation dynamics and transformation kinetics of deeply supercooled water: temperature, pressure, doping, and proton/deuteron isotope effects. *J Chem Phys.* 147:034506.
- 46 Mishima O, Calvert LD, Whalley E. 1984. ‘Melting ice’ I at 77 K and 10 kbar: a new method of making amorphous solids. *Nature.* 310:393–395.
- 47 Kohl I, Mayer E, Hallbrucker A. 2000. Thermal properties of metastable ice XII. *J Phys Chem B.* 104:12102–12104.
- 48 Salzmann CG, Loerting T, Kohl I, Mayer E, Hallbrucker A. 2002. Pure ice IV from high-density amorphous ice. *J Phys Chem B.* 106:5587–5590.
- 49 Wagner H, Richert R. 1999. Equilibrium and non-equilibrium type β -relaxations: d-sorbitol versus o-terphenyl. *J Phys Chem B.* 103:4071–4077.